REPORT DOCUMENTATION PAGE

Form Approved OMB NO. 0704-0188

1. REPORT DATE (DD-MM-YYYY)	2. REPORT TYPE	3. DATES COVERED (From - To)
06-08-2008	Final Report	1-Jul-2007 - 31-Mar-2008

4. TITLE AND SUBTITLE

Active and Passive Control of Supersonic Wakes: Numerical Investigations using DNS and LES

5a. CONTRACT NUMBER
W911NF-07-1-0380

5b. GRANT NUMBER

5c. PROGRAM ELEMENT NUMBER
611102

6. AUTHORS
Hermann F Fasel

5d. PROJECT NUMBER

5e. TASK NUMBER

5f. WORK UNIT NUMBER

7. PERFORMING ORGANIZATION NAMES AND ADDRESSES
University of Arizona
Sponsored Project Services
888 N. Euclid, #510
Tucson, AZ 85722 -

8. PERFORMING ORGANIZATION REPORT NUMBER

9. SPONSORING/MONITORING AGENCY NAME(S) AND ADDRESS(ES)
U.S. Army Research Office
P.O. Box 12211
Research Triangle Park, NC 27709-2211

10. SPONSOR/MONITOR'S ACRONYM(S)
ARO

11. SPONSOR/MONITOR'S REPORT NUMBER(S)
52967-EG-II.1

12. DISTRIBUTION AVAILIBILITY STATEMENT
Approved for Public Release; Distribution Unlimited

13. SUPPLEMENTARY NOTES
The views, opinions and/or findings contained in this report are those of the author(s) and should not contrued as an official Department of the Army position, policy or decision, unless so designated by other documentation.

14. ABSTRACT
At supersonic speed the base drag of blunt axisymmetric bodies can makeup a substantial fraction of the total drag. A reduction of the base drag is highly desirable as it would considerably improve aerodynamic performance. We employed computational fluid dynamics for investigating transitional supersonic axisymmetric wakes at a freestream Mach number of M=2.46 and a Reynolds number based on diameter of Re_D=100,000. For these simulations, to lower the grid resolution requirement we employed a hybrid turbulence model, the flow simulation methodology. We investigated flow

15. SUBJECT TERMS
Supersonic Wakes, Axisymmetric wakes, Supersonic Base Flows, Axisymmetric Base Flows, Flow Control

16. SECURITY CLASSIFICATION OF:			17. LIMITATION OF ABSTRACT	15. NUMBER OF PAGES	19a. NAME OF RESPONSIBLE PERSON
a. REPORT	b. ABSTRACT	c. THIS PAGE			Hermann Fasel
U	U	U	SAR		19b. TELEPHONE NUMBER 520-621-2771

Report Title

Active and Passive Control of Supersonic Wakes: Numerical Investigations using DNS and LES

ABSTRACT

At supersonic speed the base drag of blunt axisymmetric bodies can makeup a substantial fraction of the total drag.
A reduction of the base drag is highly desirable as it would considerably improve aerodynamic performance.
We employed computational fluid dynamics for investigating transitional supersonic axisymmetric wakes at a freestream Mach number of M=2.46 and a Reynolds number based on diameter of Re_D=100,000. For these simulations, to lower the grid resolution requirement we employed a hybrid turbulence model, the flow simulation methodology. We investigated flow control mechanisms that alter the near wake by introducing time-periodic and steady, axisymmetric and longitudinal perturbations into the approach boundary layer. The objective of our research was to understand how the various active and passive flow control techniques affect the flow dynamics, in particular the low wave number azimuthal modes which in our earlier research was found to be primarily responsible for the low base pressure. We also investigated passive control using steady basebleed.

List of papers submitted or published that acknowledge ARO support during this reporting period. List the papers, including journal references, in the following categories:

(a) Papers published in peer-reviewed journals (N/A for none)

Sivasubramanian, J., Sandberg, R. D., von Terzi, D. A., and Fasel, H. F., "Numerical Investigation of Transitional Supersonic Base Flows with Flow Control," Journal of Spacecraft and Rockets, Vol. 44, No. 5, 2007, pp. 1021-1028.

Number of Papers published in peer-reviewed journals: 1.00

(b) Papers published in non-peer-reviewed journals or in conference proceedings (N/A for none)

Number of Papers published in non peer-reviewed journals: 0.00

(c) Presentations

Number of Presentations: 0.00

Non Peer-Reviewed Conference Proceeding publications (other than abstracts):

Number of Non Peer-Reviewed Conference Proceeding publications (other than abstracts): 0

Peer-Reviewed Conference Proceeding publications (other than abstracts):

Sivasubramanian, J., and Fasel, H. F., "Numerical Investigation of Supersonic Axisymmetric Wakes with Active and Passive Flow Control," 4th Flow Control Conference, June 23-26, 2008, AIAA Paper No. 2008-3999.

Number of Peer-Reviewed Conference Proceeding publications (other than abstracts): 1

(d) Manuscripts

Number of Manuscripts: 0.00

Number of Inventions:

Graduate Students

NAME	PERCENT_SUPPORTED
Jayahar Sivasubramanian	0.50
FTE Equivalent:	**0.50**
Total Number:	**1**

Names of Post Doctorates

NAME	PERCENT_SUPPORTED
FTE Equivalent:	
Total Number:	

Names of Faculty Supported

NAME	PERCENT_SUPPORTED	National Academy Member
Hermann F Fasel	0.04	No
FTE Equivalent:	**0.04**	
Total Number:	**1**	

Names of Under Graduate students supported

NAME	PERCENT_SUPPORTED
FTE Equivalent:	
Total Number:	

Student Metrics

This section only applies to graduating undergraduates supported by this agreement in this reporting period

The number of undergraduates funded by this agreement who graduated during this period:	0.00
The number of undergraduates funded by this agreement who graduated during this period with a degree in science, mathematics, engineering, or technology fields:.....	0.00
The number of undergraduates funded by your agreement who graduated during this period and will continue to pursue a graduate or Ph.D. degree in science, mathematics, engineering, or technology fields:.....	0.00
Number of graduating undergraduates who achieved a 3.5 GPA to 4.0 (4.0 max scale):	0.00
Number of graduating undergraduates funded by a DoD funded Center of Excellence grant for Education, Research and Engineering:	0.00
The number of undergraduates funded by your agreement who graduated during this period and intend to work for the Department of Defense	0.00
The number of undergraduates funded by your agreement who graduated during this period and will receive scholarships or fellowships for further studies in science, mathematics, engineering or technology fields:	0.00

Names of Personnel receiving masters degrees

NAME
Total Number:

Names of personnel receiving PHDs

NAME
Total Number:

Names of other research staff

NAME	PERCENT_SUPPORTED
FTE Equivalent:	
Total Number:	

Sub Contractors (DD882)

Inventions (DD882)

Final Report

ARO-STIR Grant No. W911NF0710380

Active and Passive Control of Supersonic Wakes: Numerical Investigations using DNS and LES

by

Hermann F Fasel

Department of Aerospace and Mechanical Engineering

The University of Arizona

Tucson, AZ 85721

Submitted to

Dr. Thomas L. Doligalski, chief

Fluid Dynamics Branch

Engineering Sciences Division

U.S. Army Research Office

J u n e 2 0 0 8

Table of Contents

Nomenclature

A = amplitude

A_{dist} = disturbance amplitude

c_p = pressure coefficient

c_T = coefficient for turbulent timescale

c_v = specific heat

δ_{ik} = Kronecker symbol

Δ = grid line spacing

ε = turbulent dissipation rate

E = total energy $E = c_v T + \frac{1}{2} u_i u_i$

$f_{\varepsilon 2}$ = wall damping function

$f(\Delta / L_k)$ = contribution function

γ = ratio of specific heats

I = dimensionless injection parameter

k = azimuthal Fourier mode number

kh = total number of azimuthal Fourier modes

K = turbulent kinetic energy

L_K = Kolmogorov length scale

μ = dynamic viscosity

μ_T = turbulent eddy viscosity

M, M_T = Mach number, turbulent Mach number

p = pressure

Π = source term

Pr, Pr_T = Prandtl number, turbulent Prandtl number

Q_k = turbulent heat flux

q_k = heat-flux vector

Re = Reynolds number

ρ = density

S_{ij} = strain-rate tensor

σ_{ij} = subgrid stress-tensor

τ_{ik} = stress tensor

T = temperature

u_i = velocity vector

W_{ik} = vorticity tensor

z, r, θ = streamwise, radial and azimuthal coordinate

$\overline{\phi}$ = Reynolds average of ϕ

$\widetilde{\phi}$ = Favre average of ϕ

Subscripts

D = quantity based on diameter of cylinder

i, j, k = indices for Cartesian tensor notation

T = turbulent

Superscripts

R = resolved

k = k^{th} mode of quantity

Abstract

At supersonic speed the base drag of blunt axisymmetric bodies can makeup a substantial fraction of the total drag. A reduction of the base drag is highly desirable as it would considerably improve aerodynamic performance. We employed computational fluid dynamics for investigating transitional supersonic axisymmetric wakes at a freestream Mach number of $M = 2.46$ and a Reynolds number based on diameter of $Re_D = 100,000$. For these simulations, to lower the grid resolution requirement we employed a hybrid turbulence model, the flow simulation methodology. We investigated flow control mechanisms that alter the near wake by introducing time-periodic and steady, axisymmetric and longitudinal perturbations into the approach boundary layer. The objective of our research was to understand how the various active and passive flow control techniques affect the flow dynamics, in particular the low wave number azimuthal modes which in our earlier research was found to be primarily responsible for the low base pressure. We also investigated passive control using steady basebleed.

1. Introduction

In supersonic flight of axisymmetric aerodynamic bodies with a blunt base such as missiles, rockets, and projectiles, the base drag has a considerable effect on the total aerodynamic drag. A schematic of the mean flow field is shown in Figure 1.1. The supersonic approach boundary layer (1) separates at the base and undergoes an expansion (2) with a large turning angle, causing a strong reduction in pressure. A free shear layer (3) forms, separating the outer inviscid fluid from a large recirculation region (4) downstream of the base. As the free shear layer approaches the axis of symmetry, a recompression process (5) occurs that realigns the flow with the axis and subjects the shear layer to a strong adverse pressure gradient. The location where the mean axial velocity at the axis is zero (6) separates the region of reverse flow from the trailing wake (7). Depending on the shape and extent of the recirculating flow region, some pressure may be recovered at the base. However, in general the base pressure is considerably lower than the stagnation pressure which result in base drag. In fact, in flight tests with U.S. Army projectiles [1] it was found that the base drag can be up to 35% of the total drag. Experimental as well as numerical investigations indicate that by modifying the recirculating flow that develops in the near wake region, the base pressure and therefore the overall performance of the flight vehicle can be altered. For this reason, in the past, numerous research efforts, experimental,

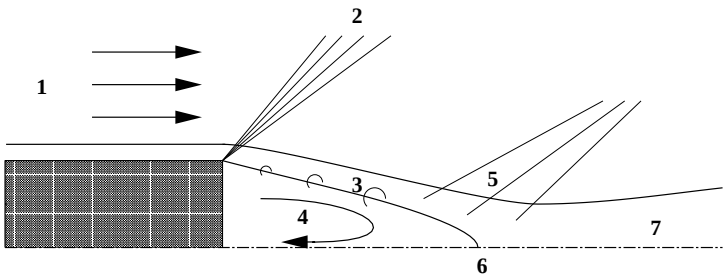

Figure 1.1 Schematic of mean flow field.

theoretical, and computational, have focused on understanding the flow physics and on deriving methods for altering or controlling the near-wake flow dynamics such that the base pressure increased. The near-wake can be modified by passive techniques such as basebleed, boat-tailing, base-burning etc. or, unsteady forcing which is referred to as active flow control. Active flow control that exploits flow instabilities can potentially be very effective requiring only a minimal control effort.

Sandberg and Fasel [2, 3, 4] employed both, spatial and temporal Direct Numerical Simulations to study the near-wake region of supersonic axisymmetric wakes at $M = 2.46$ and Reynolds numbers between $30,000$ and $100,000$. These simulations provided insight into the hydrodynamic instability mechanisms that lead to the formation of large coherent structures which were found to decrease the base pressure and then increase the base drag. The existence of such large coherent structures in supersonic axisymmetric wakes was confirmed experimentally by Bourdon and Dutton [5, 6]. We conjectured that by influencing the strength and dynamics of the coherent structures the base pressure could be affected and thus, ultimately the base drag be reduced. We also concluded that the key to an effective flow control technique was to understand and exploit the instability mechanisms that govern the dynamics of the (coherent) turbulent flow structures.

Sandberg and Fasel [2] concluded that the azimuthal modes $k = 1, 2, 3, 4$ are the dominant modes for supersonic axisymmetric wakes. In particular, mode $k = 2$ is responsible for a "four-lobe" wake structure of the meanflow and significant entrainment of fluid from the recirculation region, and, consequently, a low base-pressure. The knowledge gained from these calculations motivated the use of flow control methods to exploit and/or counteract the instability mechanisms present in the flow, such that a base pressure increase, and, consequently, a drag reduction could be accomplished. Direct Numerical Simulations (DNS) performed for $M = 2.46$ and $Re_D = 30,000$ by Sivasubramanian *et al.* [7] showed that by weakening the dominance of the low-wavenumber modes, the base pressure could be increased.

Direct Numerical Simulations of supersonic axisymmetric wakes at Reynolds numbers in the order of $\mathcal{O}(10^6)$, as in the experiments at UIUC, with sufficient resolution in space and time are out of reach even with todays supercomputers. Alternative simulation approaches for computing such flows have to be considered, such as Reynolds Averaged Navier-Stokes (RANS) and Large Eddy Simulation (LES). Unfortunately, RANS models often fail to provide accurate results for unsteady separated flows. Because of its ability to capture three-dimensional unsteady flow structures, LES would be the method of choice. However at high Reynolds numbers the LES resolution requirements are still prohibitively high. As an alternative, hybrid methods, which combine the advantages of DNS, LES, and RANS into one model may be considered. Supersonic axisymmetric wake simulation with hybrid turbulence models were carried out by e.g. Forsythe *et al.*, [8] Sandberg & Fasel, [9] and Kawai *et al.* [10].

For the present investigation of supersonic wakes at $M = 2.46$ and $Re_D = 100,000$ a hybrid method, the Flow Simulation Methodology (FSM) was employed. We investigated how unsteady actuation of the axisymmetric mode and steady forcing of the higher azimuthal modes affects the base pressure. The former excites the kelvin-helmholtz instability while the latter introduces steady streamwise vortical structures. We also investigated the effect of steady basebleed.

2. Governing Equations

The fluid is assumed to be an ideal gas with constant specific heat coefficients. All quantities are made dimensionless using the free-stream conditions. The radius of the body was chosen as reference length. Applying a filter to the governing equations yields the resolved continuity, momentum, and energy equations as:

$$\frac{\partial \overline{\rho}}{\partial t} + \frac{\partial}{\partial x_k}\left(\overline{\rho}\widetilde{u}_k\right) = 0 \ , \tag{2.1}$$

$$\frac{\partial}{\partial t}\left(\overline{\rho}\widetilde{u}_i\right) + \frac{\partial}{\partial x_k}\left[\overline{\rho}\widetilde{u}_i\widetilde{u}_k + \overline{p}\delta_{ik} - \left(\overline{\tau}_{ik} - \overline{\rho}\sigma_{ik}\right)\right] = 0 \ , \tag{2.2}$$

$$\frac{\partial}{\partial t}\left(\overline{\rho}E_R\right) + \frac{\partial}{\partial x_k}\left[\overline{\rho}\widetilde{u}_k H + \overline{q}_k + Q_k - \widetilde{u}_i\left(\overline{\tau}_{ik} - \overline{\rho}\sigma_{ik}\right)\right] = \Pi \, , \tag{2.3}$$

The resolved pressure is obtained from the equation of state

$$\overline{p} = \frac{\overline{\rho}\widetilde{T}}{\gamma M^2} \, , \tag{2.4}$$

with $\gamma = 1.4$. The resolved heat flux is computed from

$$\overline{q}_k = -\frac{\kappa}{(\gamma-1)M^2 Pr Re}\frac{\partial \widetilde{T}}{\partial x_k} \, , \tag{2.5}$$

with $Pr = 0.7$.

The above equations contain three terms that do not occur in the unfiltered equations: the subgrid stress tensor σ_{ik}, the subgrid heat-flux vector Q_k and the source term Π in the energy equation. These terms have to be modeled. For a DNS, where all time- and length-scales are resolved, the subgrid terms are zero, implying that $\phi = \overline{\phi} = \widetilde{\phi}$. In the other limit, when the filter-width is so large that all fluctuations are filtered out, a traditional RANS is recovered. For the present simulations the FSM was based on the $K - \varepsilon$ turbulence model in combination with the explicit algebraic Reynolds stress model (EASM) by Rumsey *et al.* [11].

We solved transport equation for the turbulent kinetic energy K and the turbulent dissipation rate ε.

$$\begin{aligned} \frac{\partial}{\partial t}\left(\overline{\rho}K\right) + \frac{\partial}{\partial x_k}\left[\overline{\rho}\widetilde{u}_k K - \left(\frac{\overline{\mu}}{Re} + \frac{\mu_T}{\sigma_K}\right)\frac{\partial K}{\partial x_k}\right] &= \Pi_K\,, \qquad (2.6) \\ \frac{\partial}{\partial t}\left(\overline{\rho}\varepsilon\right) + \frac{\partial}{\partial x_k}\left[\overline{\rho}\widetilde{u}_k \varepsilon - \left(\frac{\overline{\mu}}{Re} + \frac{\mu_T}{\sigma_\varepsilon}\right)\frac{\partial \varepsilon}{\partial x_k}\right] &= \Pi_\varepsilon\,. \qquad (2.7) \end{aligned}$$

The turbulent viscosity μ_T is given as

$$\mu_T = c_\mu \tau_T K\,, \qquad (2.8)$$

with $c_\mu = 0.09$. The additional constants that appear in the turbulent diffusion terms are $\sigma_K = 1.0$ and $\sigma_\varepsilon = 1.3$.

Source Terms

The source terms that appear in the energy and turbulence model equation include a pressure dilatation term, terms involving the turbulent dissipation rate and the subgrid mass-flux. It was shown by Sarkar *et al.* [12] that both pressure dilatation and compressible dissipation are important in compressible turbulence. Therefore, both effects are modelled according to Sarkar *et al.* [12], Sarkar [13] and Speziale [14] by computing the source terms as

$$\begin{aligned} \Pi &= \left(1 - a_2 M_T\right)\overline{\rho}\sigma_{ik}\widetilde{S}_{ik} + \left(1 - a_3 M_T^2\right)\bar{\rho}\varepsilon - \left(\overline{\tau}_{ik} - \bar{p}\delta_{ik}\right)\frac{\partial}{\partial x_k}\left[\frac{\mu_T}{\sigma_\rho}\frac{\partial}{\partial x_i}\left(\frac{1}{\bar{\rho}}\right)\right]\,, \\ \Pi_K &= -\left(1 - a_2 M_T\right)\overline{\rho}\sigma_{ik}\widetilde{S}_{ik} - \left(1 - a_3 M_T^2\right)\bar{\rho}\varepsilon - \left(\frac{\partial p}{\partial x_i} - \frac{\partial \tau_{ik}}{\partial x_k}\right)\frac{C_\mu}{\overline{\rho}\sigma_\rho}\tau K\frac{\partial \overline{\rho}}{\partial x_i}\,, \qquad (2.9) \end{aligned}$$

$$\Pi_\varepsilon = -C_{\varepsilon 1}\overline{\rho}\frac{1}{\tau_T}\sigma_{ik}\left(\frac{\partial \widetilde{u}_i}{\partial x_k} - \frac{1}{3}\widetilde{S}_{jj}\delta_{ik}\right) - C_{\varepsilon 2}f_{\varepsilon_2}\overline{\rho}\frac{\varepsilon}{\tau_T} + C_{\varepsilon 3}\bar{\rho}Re_T^{\frac{1}{2}}\frac{\varepsilon}{\tau_T} - \frac{4}{3}\bar{\rho}\varepsilon\widetilde{S}_{jj}\,, \qquad (2.10)$$

with the constants $\sigma_\rho = 0.5$, $a_2 = 0.15$, $a_3 = 0.2$, $C_{\varepsilon 1} = 1.44$, $C_{\varepsilon 2} = 1.83$, and $C_{\varepsilon 3} = 0.001$. Here $f_{\varepsilon 2}$ is a wall-damping function, and Re_T is the turbulent Reynolds number

$$Re_T = \frac{\overline{\rho} K}{\overline{\mu}} \tau_T \,. \tag{2.11}$$

To remove singularities at walls in the destruction term of the ε-equation, i.e., $K = 0$, a damping function $f_{\varepsilon 2}$ is used. Traditionally, this wall-damping function takes the form

$$f_{\varepsilon 2}(N) = 1 - exp\left(-Re\sqrt{0.1K}N\right) \;, \tag{2.12}$$

where N is the wall-normal distance. In the EASM model implemented here, this wall-damping function is the only term containing the wall-distance; the Reynolds stress model automatically accounts for near-wall effects through the computation of α_1/τ. To be completely independent of the wall-distance, we employed another approach which is based on suggestion by Durbin [15] for computing $f_{\varepsilon 2}$. By computing $f_{\varepsilon 2}$ as

$$f_{\varepsilon 2} = \frac{1}{max\left[1, \frac{C_T}{\sqrt{Re_T}}\right]} \;, \tag{2.13}$$

it is assumed that the turbulent time scale is limited by the Kolmogorov time-scale. The additional constant C_T was calibrated by Sandberg [16].

3. Flow Simulation Methodology

The Flow Simulation Methodology (FSM) is a hybrid turbulence model that was designed to provide the proper amount of modeling based on the local and instantaneous physical resolution. The amount of modeling is determined by a contribution function which locally and instantaneously compares the smallest relevant turbulent length scales to the local grid resolution. The contribution function is designed such that no modeling is provided in the DNS limit when the physical resolution is such that all scales of motion are resolved. In the coarse-grid limit all scales of motion are modeled and, the FSM reverts to a full RANS. In between these resolution limits, a LES recovered where the subgrid stress is obtained from the underlying turbulence model.

For the Flow Simulation Methodology, the turbulent stress tensor is multiplied by the contribution function $f(\Delta/L_k)$

$$\sigma_{ik} = f(\Delta/L_k)\,\sigma_{ik}^R\,. \tag{3.1}$$

For the compressible extension,[17, 18] the source term in the energy equation and the turbulent heat-flux vector have to be rescaled with the same contribution function:

$$Q_k = f(\Delta/L_k)\,Q_k^R \quad \text{and} \quad \Pi = f(\Delta/L_k)\,\Pi^R. \tag{3.2}$$

The term $\Delta = [(\Delta z^2 + \Delta r^2 + (r\Delta\theta)^2)/3]^{1/2}$ is the local grid-line spacing and L_k is the Kolmogorov length-scale, $L_k = (\mu/\rho Re)^{3/4}/\epsilon^{1/4}$. For the present simulations, a contribution function proposed by Speziale[17] was employed

$$f(\Delta/L_k) = \left(1 - e^{-\beta\frac{\Delta}{L_k}}\right)^n\,, \tag{3.3}$$

where β and n are adjustable parameters. Following Speziale[17], n is set to unity and β is set to a small value of the order of $\mathcal{O}(10^{-3})$. Other forms of the contribution function and different choices of the length-scale are possible [19].

4. Numerical Method

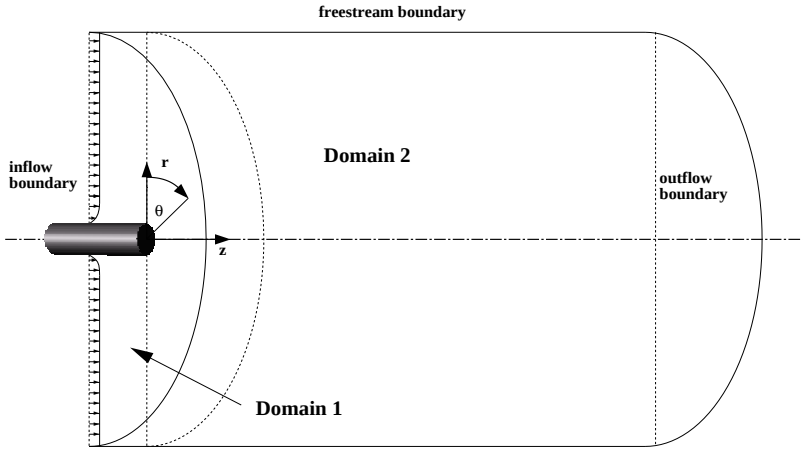

Figure 4.1 Computational domain.

The compressible Navier-Stokes equations in cylindrical coordinates are solved using sixth-order accurate split compact differences in the radial direction, fourth-order accurate split differences in the streamwise direction, and a pseudospectral discretization in the azimuthal direction. To preserve accuracy, the finite differences were derived for non-equidistant grids. A state-of-the-art axis treatment is implemented, exploiting parity conditions [20]. For the time advancement, a standard fourth-order Runge-Kutta scheme is employed. The Reynolds stresses are also computed with a high-order accurate scheme. Only the density gradients are computed with a second-order accurate difference approximations for introducing numerical dissipation in areas where shocks and expansion waves are present in the flow.

A sketch of the computational domain is shown in Figure 4.1. Only one half of the entire flow was computed assuming symmetry of the flow. Dirichlet and Neumann conditions, respectively were applied at the inflow and outflow boundaries. It was

assumed that the approach flow was laminar. Therefore, the contribution function was manually set to zero in the approach flow, such that the approach boundary layer remained laminar. In addition, K was set to zero at the inflow boundary to be consistent with the laminar approach-flow assumption.

5. Flow Control Techniques

One of the many passive means for modifying the near wake flow and, hence, the base pressure are vortex generators. In the present investigation vortex generators are modeled, by introducing steady disturbances into the approach boundary layer, just upstream of the base (center of disturbances at $r = 1.05$, $z = -0.15$) by a steady volume force $\hat{F}^k_{VF}$. The volume force was added to the right-hand-side (RHS) of the radial momentum equation in Fourier space, such that a specific azimuthal mode could be forced with a disturbance amplitude A_{dist}. The disturbances can also be periodic in time with a frequency ω for active flow control.

The volume force was computed as

$$\hat{F}^k_{VF} = A_{dist} \sin(2\pi\omega t) \left[1 - \cos\left(\frac{(r - r_b)\pi}{r_e - r_b}\right)\right] \left[1 - \cos\left(\frac{(z - z_b)\pi}{z_e - z_b}\right)\right] , \qquad (5.1)$$

where k denotes the azimuthal mode that is being forced, and r_b, r_e, z_b and z_e denote the start and end points of the forcing "blob" in the radial and streamwise directions, respectively.

Two different forcing mechanisms (steady or unsteady) for altering the near-wake were investigated:

1. By emulating vortex generators using steady disturbances, longitudinal vortices were introduced into the initial shear-layer, imposing symmetries on the flow in the $r - \theta$ plane and reducing the strength of helical modes with low mode-numbers.

2. Axisymmetric periodic perturbations were introduced, which, due to compressibility effects, do not experience significant amplification in the streamwise direction, but should reduce the energy transfer from the mean flow to the oblique structures, thereby decreasing the growth of helical instability modes.

We also investigated passive control of the supersonic wake using a central bleed jet. The setup was similar to the experiments by Mathur and Dutton[21, 22] but the Reynolds number was maintained at $Re_D = 100,000$. In the experiments, magnitude of the bleed flow rate was quantified using a non-dimensional injection parameter, I, defined as the bleed mass flow rate normalized by the product of the base area and the product of freestream velocity and density. This definition of the injection parameter does not account for the approach boundary-layer thickness and the bleed flow momentum, both of which have been shown to affect the base pressure in a manner analogous to basebleed. For the basebleed, a Dirichlet boundary condition was employed for generating the bleed jet.

6. Results

6.1 Natural Wake

We performed FSM simulations of transitional axisymmetric supersonic wakes at $Re_D = 100,000$ and $M = 2.46$. The computational grid had 452 and 90 points in the streamwise and the radial direction, respectively. We conducted simulations with $kh = 32$ and 16 azimuthal Fourier modes (kh is the total number of Fourier modes used in a simulation). As initial condition for the FSM simulations, the axisymmetric RANS data from Sandberg [16] was used and the desired number of azimuthal Fourier modes were added. We then added a pulse disturbance to the higher Fourier modes of the density in order to initiate the three-dimensional motion. We first simulated the uncontrolled flow and compared our FSM results with earlier DNS data by Sandberg and Fasel [3, 4].

Figures 6.1a-d show sideviews of the instantaneous vorticity magnitude obtained from simulations with $kh = 16$ and 32 azimuthal modes and different values of β.

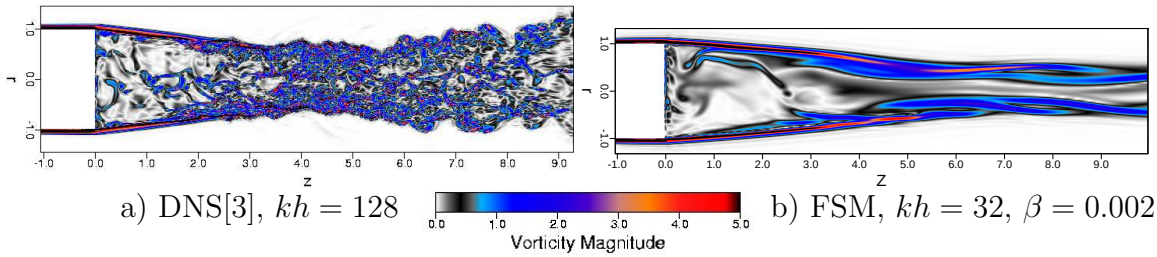

a) DNS[3], $kh = 128$ b) FSM, $kh = 32$, $\beta = 0.002$

c) FSM, $kh = 32$, $\beta = 0.004$ d) FSM, $kh = 16$, $\beta = 0.004$

Figure 6.1 Sideviews of contours of instantaneous total vorticity magnitude for natural uncontrolled wake

Figure 6.2 Instantaneous iso-contours of $Q = 0.05$ from FSM calculations using $kh = 32$ & $\beta = 0.002$ (top) and $kh = 16$ & $\beta = 0.004$ (bottom); perspective view from inflow towards outflow; base of body shaded grey.

For reference, DNS data of Sandberg and Fasel[3, 4] was included as well. The DNS results display a broad range of scales. For the FSM calculations, the small scale structures are modeled and therefore not visible and only some large-scale structures (on the order of the shear layer thickness) are resolved. Also, the widening of the wake as observed in the DNS for $z > 5$ is not captured. This could be attributed to the coarse grid resolution which puts too much burden on the hybrid model in the trailing wake region. However, within the recirculation region and the initial shear layer the model contribution is very low, allowing for the formation of flow

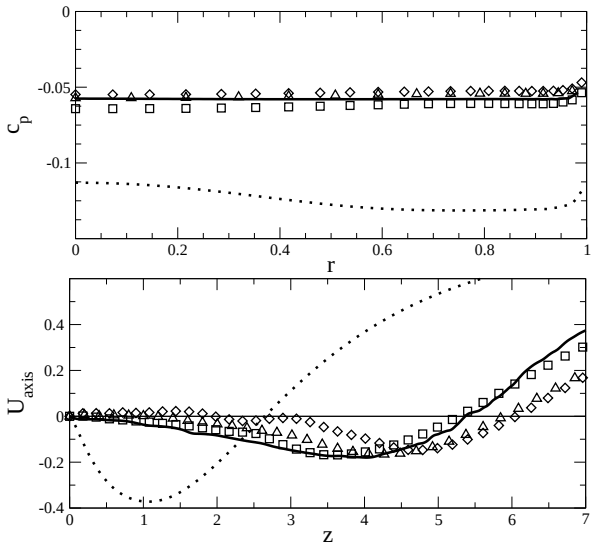

Figure 6.3 Pressure coefficient on base (top) and streamwise velocity along axis of symmetry (bottom) for natural wake; DNS, $kh = 128$ (solid curve), axisymmetric RANS (dotted curve), FSM, $kh = 32$, $\beta = 0.002$ ($\diamond$), FSM, $kh = 32$, $\beta = 0.004$ ($\triangle$), FSM, $kh = 16$, $\beta = 0.004$ ($\square$).

structures as seen in Figure 6.2. In this figure, the coherent structures were identified by considering iso-surfaces of the second invariant of the velocity gradient tensor, the "$Q - criterion$"[23]. In both cases, FSM qualitatively reproduces the flow features observed in the DNS [3, 4]. Axisymmetric structures can be observed in the shear layer close to the base. Additionally, a large number of longitudinal structures can be seen within the recirculation region, which are a consequence of the helical structures. Hairpin vortices can be observed downstream of the recompression region.

To allow for a more quantitative comparison of the different results, the time-averaged streamwise velocity along the axis of symmetry and the time-averaged pressure coefficient on the base are shown in Figure 6.3. The data for DNS and the axisymmetric RANS calculation which are used as initial condition are included for reference. In contrast to the axisymmetric RANS calculations, the pressure distribution obtained from the FSM computations is practically flat, and close to the pressure distribution obtained from the DNS. When the number of azimuthal Fourier modes

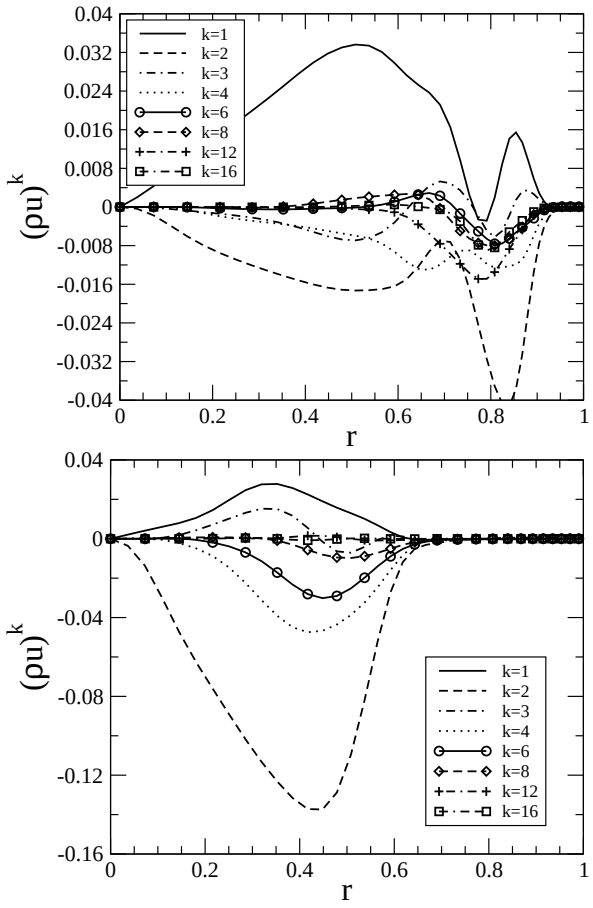

Figure 6.4 Time-averaged radial profiles of azimuthal Fourier modes of (ρu) obtained from FSM simulation of natural wake using $kh = 16$ & $\beta = 0.004$; $z = 2.5$ (top), $z = 7$ (bottom).

is increased from 16 to 32, almost the same mean base pressure profile as in the DNS is obtained and the streamwise axis-velocity distribution differs only slightly. It can also be seen that the dependence of the solution on the modelling parameter β is not very strong. This implies that the model contribution for both β is satisfactory. The value of β which leads to the best agreement with the DNS data is 0.004, which is similar to the value that resulted in the best match for lower Reynolds number calculations [24]. Results from FSM calculations with various azimuthal resolution and β were qualitatively similar. Therefore, all simulations where we investigated

passive and active flow control were carried out using FSM with 16 azimuthal modes and $\beta = 0.004$.

The amplitude distributions of the azimuthal modes of the time-averaged streamwise velocity component for two different downstream locations were extracted from the FSM simulation with $kh = 16$ and $\beta = 0.004$ and are shown in Figure 6.4. One location ($z = 2.5$) is upstream of the recompression region, where considerable reverse-flow occurs. The second location ($z = 7$) is within the far wake. The streamwise velocity component was chosen since it contains most of the energy. It can be observed that the first and second azimuthal modes have high amplitudes at both locations. At $z = 2.5$ mode $k = 1$ has the highest amplitude within the recirculation region and mode $k = 2$ has the highest amplitude in the shear layer. At the far wake location, mode $k = 2$ has the highest amplitude followed by mode $k = 4$. These observations are consistent with our earlier DNS results [3, 4].

6.2 Controlled Wake

6.2.1 Steady Forcing

We investigated three cases with steady forcing: forcing either mode $k = 2$, 4, or 8, thereby generating 4, 8 or 16 counter-rotating longitudinal structures in the circumferential direction. Visualizations of instantaneous isosurfaces of $Q = 0.05$ that illustrate the generation and evolution of coherent structures are shown in Figure 6.5. When steady forcing is applied to modes $k = 2$ and 4, an increased number of hairpin vortices can be seen in the trailing wake, otherwise, the flow looks similar to the unforced wake. When mode $k = 8$ is forced, longitudinal structures which are generated at the forcing location by the steady forcing, can be observed.

To allow for an evaluation of the effect of steady forcing on the mean flow, time-averaged radial profiles of several azimuthal Fourier modes of the streamwise velocity component are shown in Figure 6.6. For example, when comparing the data obtained

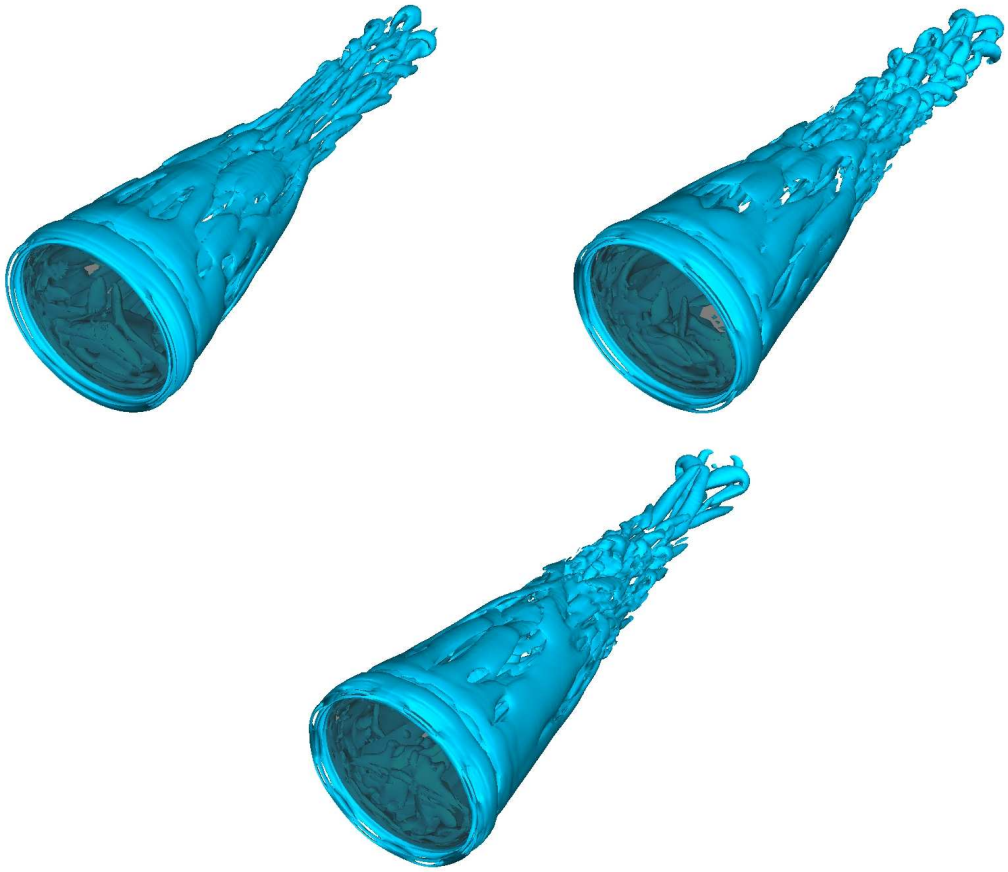

Figure 6.5 Instantaneous iso-contours of $Q = 0.05$ from FSM simulations with steady forcing; perspective view from inflow towards outflow; forcing $k = 2$ (top left), forcing $k = 4$ (top right), forcing $k = 8$ (bottom); base of body shaded grey.

from a case where mode $k = 2$ was forced with the unforced case (Figure 6.4), considerable similarity with respect to the shape and magnitude of the mode amplitude distribution can be observed for the upstream location $z = 2.5$. This may be due to the fact that mode $k = 2$ is a dominant mode in the natural wake and therefore, forcing this mode does not significantly alter the flow. However, the magnitude of mode $k = 2$ is decreased in the shear layer compared to the natural wake. Looking at the downstream location $z = 7$, the mode shape of the first azimuthal mode shows a changed radial distribution while the mode shapes of all other higher azimuthal

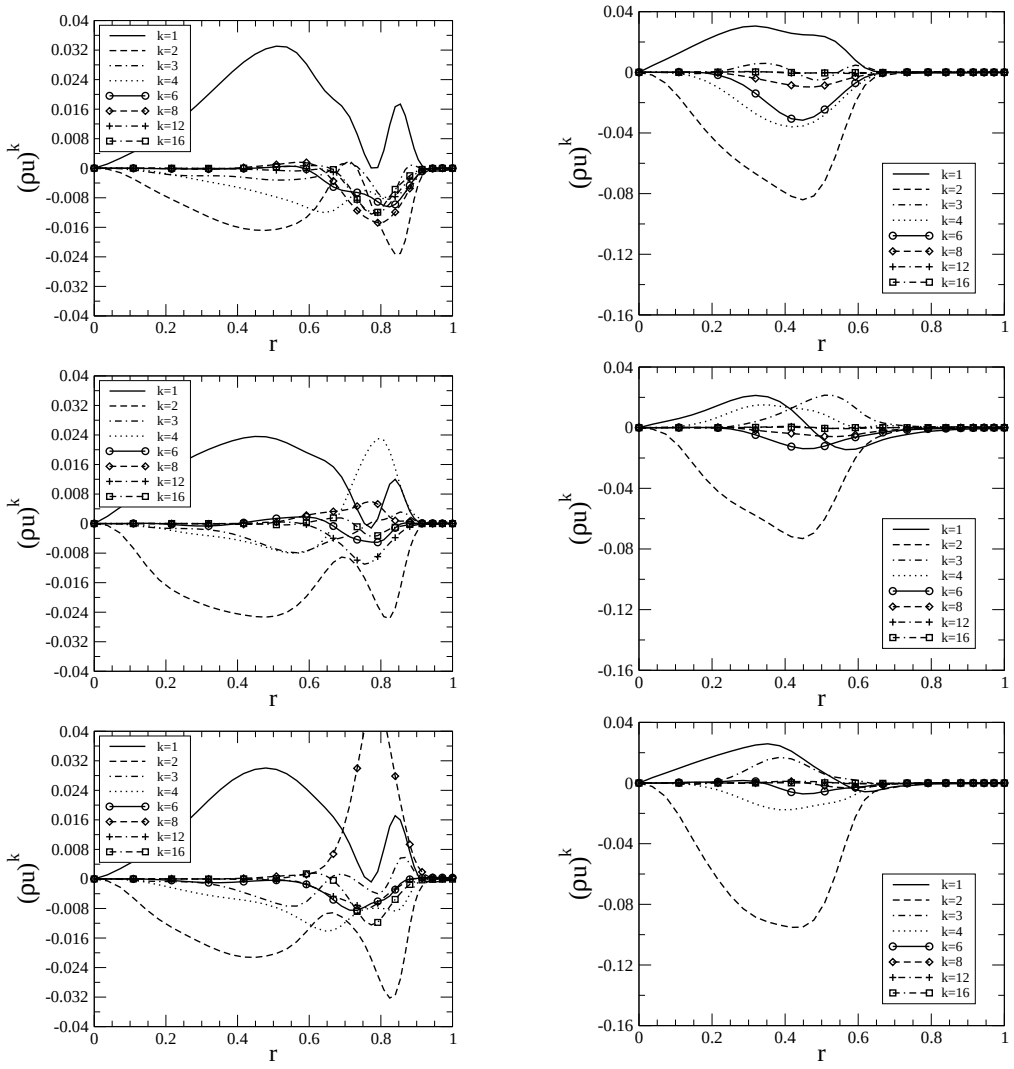

Figure 6.6 Time-averaged radial profiles of azimuthal Fourier modes of (ρu) obtained from FSM simulations with steady forcing of modes $k = 2$, $k = 4$, and $k = 8$ (from top to bottom); $z = 2.5$ (left), $z = 7$ (right).

modes resemble those found in the unforced case. However, the magnitude of modes $k = 2$, $k = 3$ and $k = 4$ are reduced. For the case where mode $k = 4$ is forced a significant peak in that mode is visible in the shear layer (at $r = 0.8$) at the upstream location, $z = 2.5$. The amplitude of modes $k = 1$ and $k = 2$ are reduced compared to the natural wake. At the downstream location $z = 7$ the amplitudes of modes $k = 2$ and $k = 4$ are reduced. When employing steady forcing of mode $k = 8$, a significant

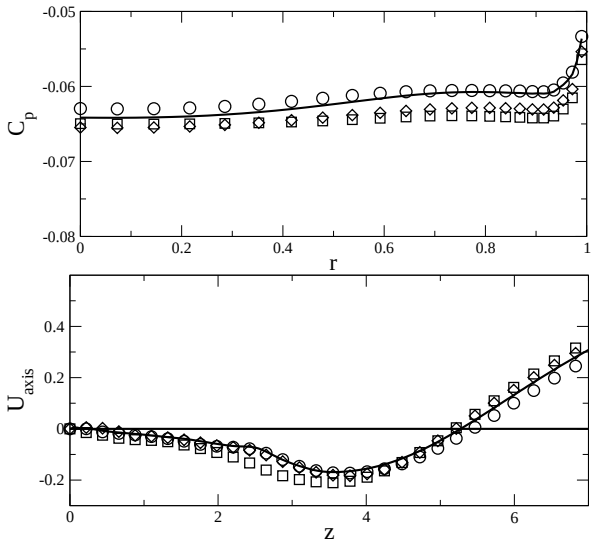

Figure 6.7 Pressure coefficient on base (top) and streamwise velocity along axis of symmetry (bottom) from FSM simulations with steady forcing; natural wake (—), forcing $k = 2$, ($\circ$), forcing $k = 4$, ($\square$), forcing $k = 8$, ($\diamond$).

peak within the shear layer is visible at the upstream location in the forced mode. For all cases with steady forcing, mode $k = 2$ is weakened. Steady forcing of modes $k = 4$ and $k = 8$ reduces the amplitude of mode $k = 1$ at $z = 2.5$. It should be noted here that forcing of mode $k = 8$ in a simulation with only 16 azimuthal modes does not allow for a detailed quantitative analysis of the flow response because the resolution is insufficient. These results should therefore, be considered to be of a qualitative nature only. We will repeat these cases with a larger number of azimuthal modes.

The time-averaged pressure coefficient along the base and the streamwise velocity distribution along the axis are shown in figure 6.7. For comparison, data for the uncontrolled flow was also included. When forcing mode $k = 2$, the recirculation length is slightly increased, resulting in a small pressure increase. Forcing of the higher azimuthal modes $k = 4$ and 8 shortens the recirculation length and decreases the base pressure. This is in agreement with experiments at an even higher Reynolds number by Bourdon and Dutton,[6] who did not detect any significant base pressure increase when generating longitudinal vortices by means of tabs on the axisymmetric

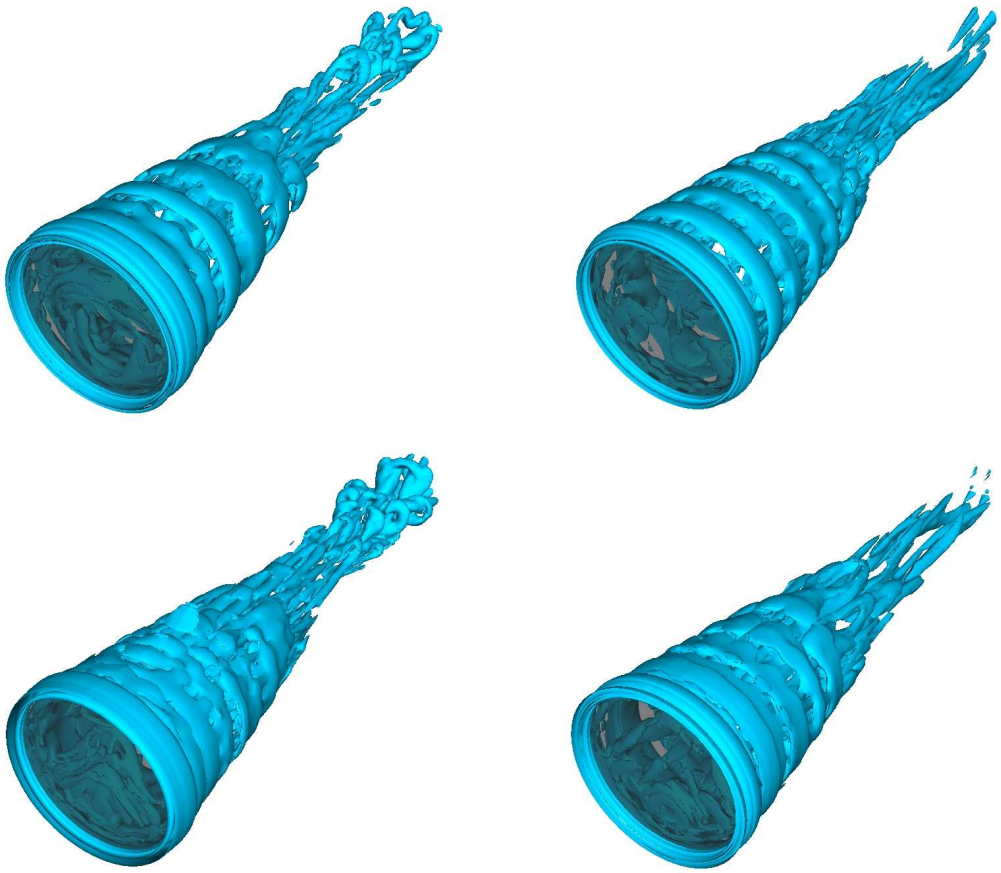

Figure 6.8 Instantaneous iso-contours of $Q = 0.05$ from FSM simulations with periodic forcing; $\omega = 1.0$ (top left), $\omega = 1.5$ (top right), $\omega = 2.0$ (bottom left) and $\omega = 2.5$ (bottom right); perspective view from inflow towards outflow; base of body shaded grey.

body.

6.2.2 Periodic Forcing

We also investigated periodic axisymmetric forcing of mode $k = 0$ for frequencies in the range $\omega = 0.4 - 2.5$. Instantaneous flow visualizations are shown in Figure 6.8. Time-periodic forcing is seen to result in the formation of axisymmetric structures in the shear layer just downstream of the base. When the axisymmetric mode was forced with frequencies $\omega = 1.0$ and $\omega = 2.0$, the flow structures far downstream from the

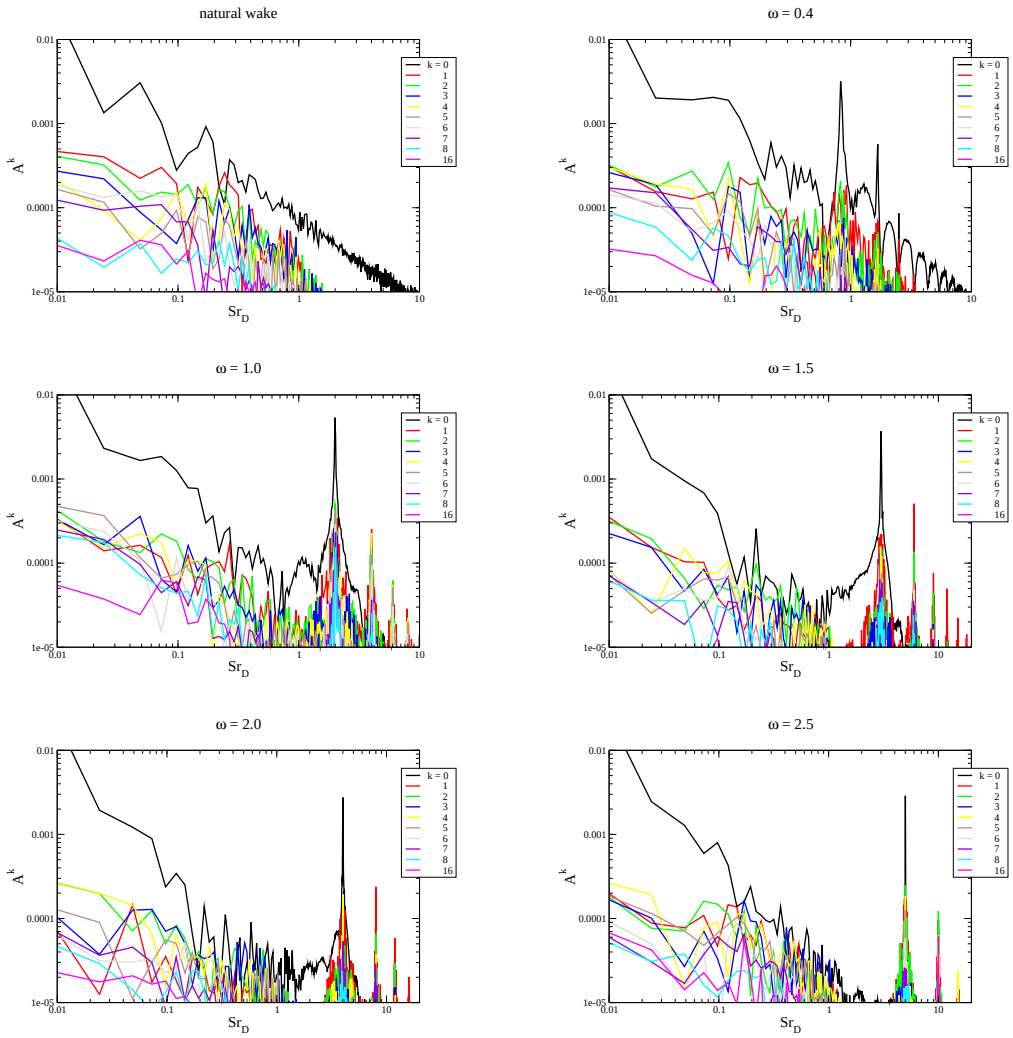

Figure 6.9 Fourier decomposition in time of higher azimuthal Fourier modes of ρ in a region of high activity for cases with periodic forcing.

base resemble those of the unforced flow. But when forcing the axisymmetric mode with frequencies $\omega = 1.5$ and $\omega = 2.5$, the hairpin vortices that are present in the trailing wake for the unforced flow disappear. We suspect that for certain frequencies (here, $\omega = 1.5$ and $\omega = 2.5$), the energy otherwise transferred to the helical structures is transferred to the axisymmetric mode, which does not exhibit significant spatial growth. The formation of hairpin vortices is suppressed as the helical modes are less energetic in these cases.

In order to identify the dominant frequencies in the flow, the azimuthal Fourier modes of density were Fourier transformed in time. Figure 6.9 shows the amplitudes of selected azimuthal modes versus the Strouhal number based on diameter for all periodic forcing cases. The dominant peaks in the spectrum are clearly related to the forcing (note that the non-dimensionalization of all quantities were performed with R as reference length whereas the Strouhal number is based on the diameter D). The spectra also show higher harmonics of the forcing frequencies.

In order to evaluate the effect of periodic forcing on the mean flow, time-averaged quantities are scrutinized. The time-averaged radial amplitude distributions of several azimuthal Fourier modes are shown in Figure 6.10 for selected periodic forcing cases. When the axisymmetric mode $k = 0$ is forced with $\omega = 1.0$. Modes $k = 1$ and $k = 2$ are suppressed at the upstream location $z = 2.5$ compared to the natural wake. At the downstream location $z = 7$, the mode $k = 2$ and $k = 4$ amplitudes are decreased while mode $k = 1$ shows a slightly higher amplitude compared to the natural wake. When mode $k = 0$ is forced with $\omega = 1.5$ the mode $k = 1$ and $k = 2$ amplitudes are again reduced in amplitude at $z = 2.5$ compared to the natural wake. But an interesting peak is obtained in mode $k = 16$ in the shear layer indicating a higher energy transfer to the unresolved scales. When the axisymmetric mode is forced with $\omega = 2.0$, at $z = 2.5$ only mode $k = 1$ experiences a slight amplitude reduction whereas mode $k = 3$ shows an increase in amplitude at $z = 7$. When mode $k = 0$ is forced with $\omega = 2.5$ the mode $k = 1$ and $k = 2$ amplitudes are reduced at $z = 2.5$. Yet,

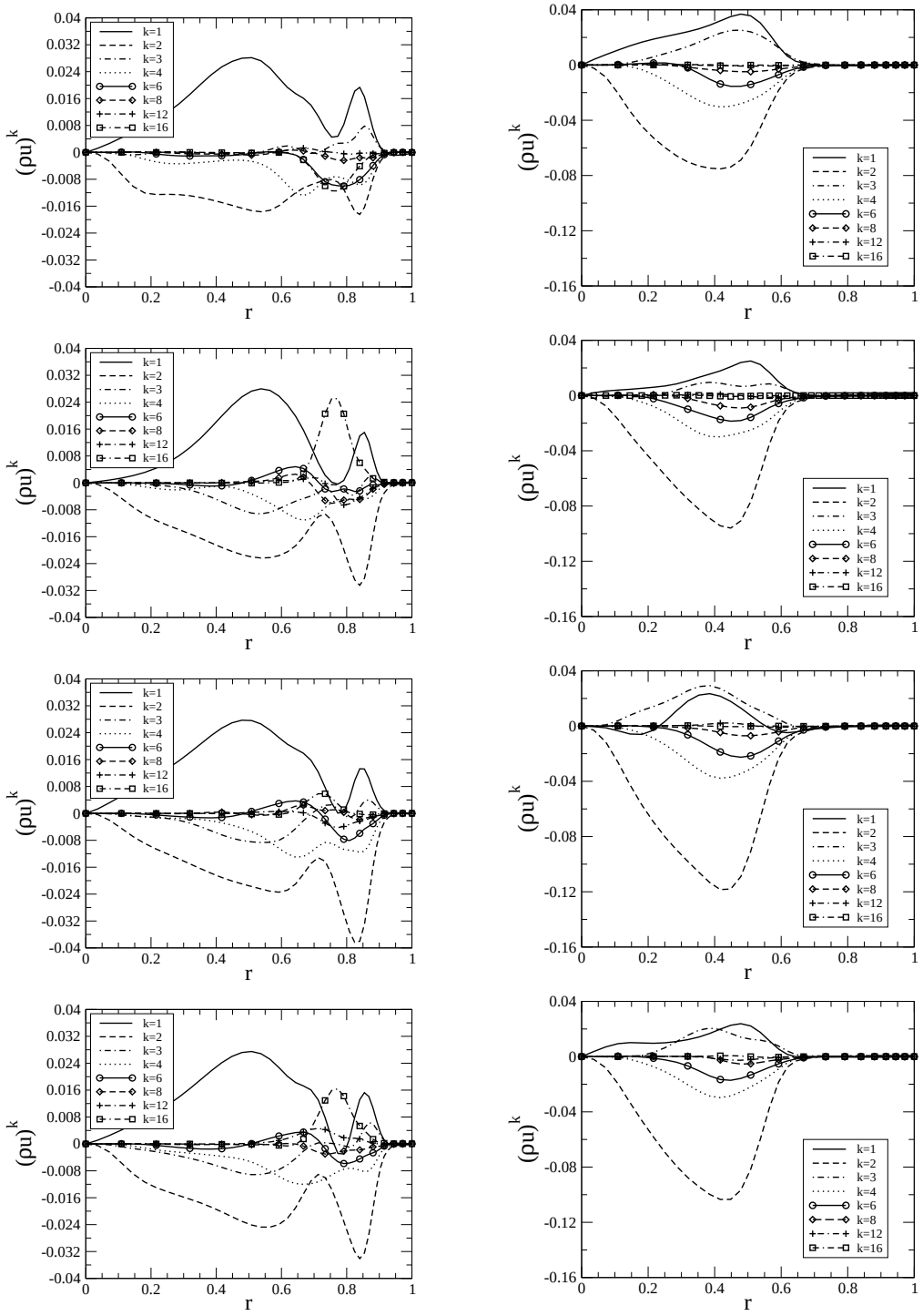

Figure 6.10 Time-averaged radial profiles of azimuthal Fourier modes of (ρu) obtained from FSM simulations with periodic forcing; $\omega = 1.0$, $\omega = 1.5$, $\omega = 2.0$, and $\omega = 2.5$ (from top to bottom); $z = 2.5$ (left), $z = 7$ (right).

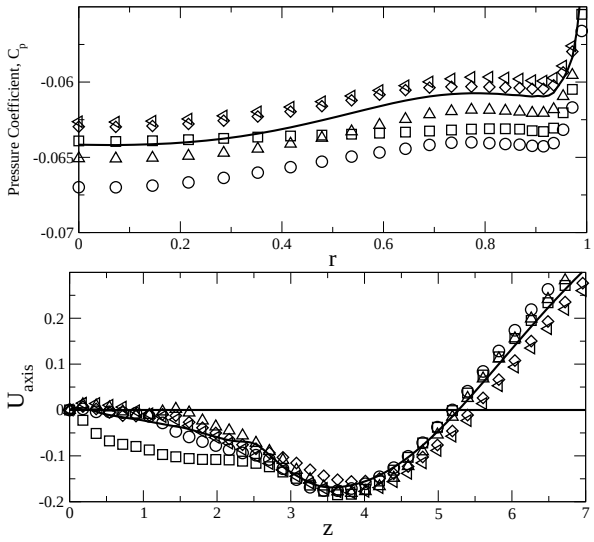

Figure 6.11 Pressure coefficient on base (top) and streamwise velocity along axis of symmetry (bottom) from FSM simulations with periodic forcing; unforced case (—), $\omega = 0.4$, ($\circ$), $\omega = 1.0$, ($\square$), $\omega = 1.5$, ($\diamond$), $\omega = 2.0$, ($\triangle$), $\omega = 2.5$, ($\triangleleft$).

again, mode $k = 16$ displays a peak in the shear layer as for the case with frequency $\omega = 1.5$. At the downstream location $z = 7$ all low wavenumber modes are reduced in amplitude compared to the natural wake.

The time-averaged streamwise velocity along the axis and the mean pressure coefficient along the base are compared in Figure 6.11. Forcing the axisymmetric mode with a low frequency of $\omega = 0.4$ results in a decrease in the recirculation length and base pressure. But as the frequency is increased to $\omega = 1.0$, both the base pressure and recirculation length increase. In fact, for $\omega = 1.5$, the base pressure is larger and recirculation length is longer than for the uncontrolled flow. When the frequency is further increased to $\omega = 2.0$ both base pressure and recirculation length are reduced compared to the natural wake. A further increase of the forcing frequency to $\omega = 2.5$ results in a further increase of both the base pressure and recirculation length. Clearly, the results are strongly dependent on the forcing frequency.

6.2.3 Basebleed

We also investigated base-bleed for various bleed flow rates. Sideviews of the instantaneous vorticity magnitude for three cases are shown in Figures 6.12a-c. The three cases belong to three distinct basebleed operating regimes. The base pressure increases fairly linearly with the bleed rate at low values of I (regime 1). A peak in the base pressure occurs at an intermediate value of I. As the bleed rate is increased past the optimum value, the base pressure decreases (regime 2) until it reaches a relative minimum. A further increase in the bleed flow leads to the onset of power-on conditions (regime 3) when the bleed flow becomes supersonic. Here, for the highest injection parameter value of $I = 0.0226$ investigated the bleed jet is still subsonic. As the injection parameter is increased the shear layer angle becomes flatter, the base corner expansion weakens, the wake widens, and the recompression shocks become weaker. Flow structures for three selected basebleed cases are shown in Figure 6.13.

Time-averaged radial amplitude distributions of several azimuthal Fourier modes of the streamwise velocity component are shown in Figure 6.14. For the low value of the injection parameter, $I = 0.0038$, compared to the natural wake, at $z = 2.5$, the mode-shape of the first azimuthal mode shows a changed radial distribution, and it has the largest amplitude of all the azimuthal modes at this location. Nevertheless, the amplitude of all modes are reduced at this location compared to the natural wake. Especially, the amplitude of mode $k = 2$ is suppressed in the shear layer. At the downstream location $z = 7$ modes $k = 2$, $k = 4$ and $k = 6$ are weakened. For the optimal injection parameter, $I = 0.0113$, mode $k = 1$ is considerably weakened by the bleed jet at the upstream location $z = 2.5$ and modes $k = 1$ and $k = 2$ are suppressed in the shear layer. All modes are suppressed at the downstream location $z = 7$ compared to the natural flow, indicating reduced growth rates in the shear layer. For the highest value of the injection parameter, $I = 0.0226$, although at $z = 2.5$ the mode $k = 1$ and $k = 2$ amplitudes seem to be reduced, further downstream at $z = 7$,

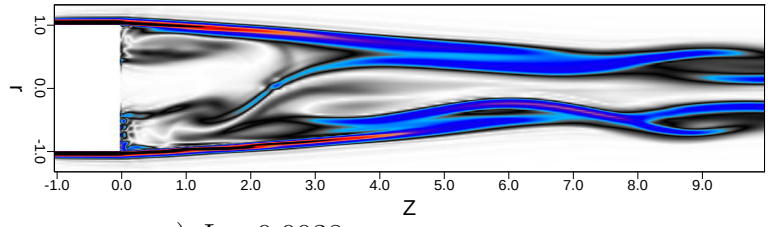

a) $I = 0.0038$

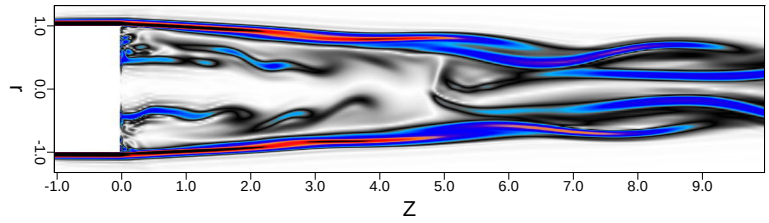

b) $I = 0.0113$

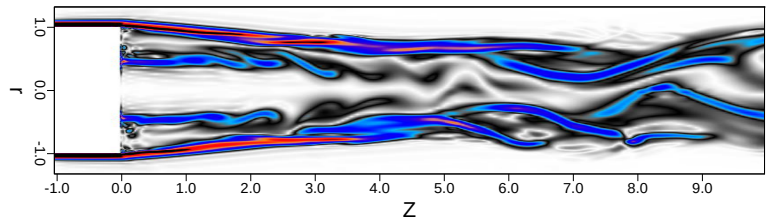

c) $I = 0.0226$

Figure 6.12 Sideviews of contours of instantaneous total vorticity for basebleed cases

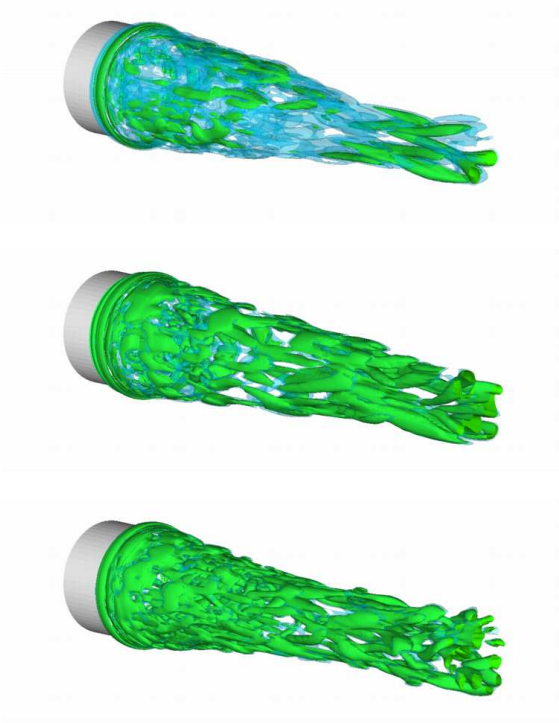

Figure 6.13 Instantaneous iso-contours of $Q = 0.1$ (green) and $Q = 0.05$ (blue) from FSM simulations with basebleed; $I = 0.0038$, $I = 0.0113$, $I = 0.0226$ (from top to bottom); perspective view with flow from left to right.

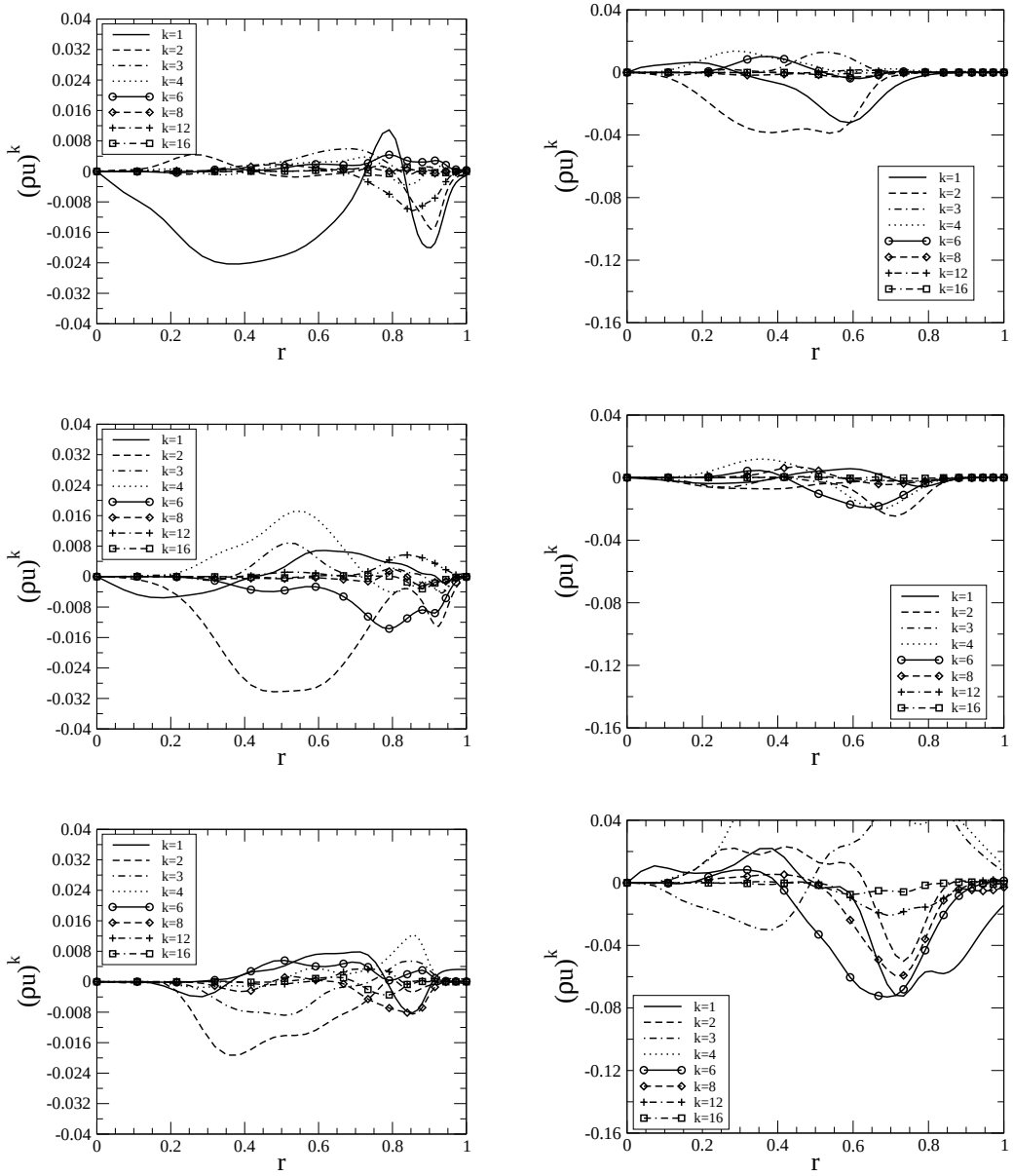

Figure 6.14 Time-averaged radial profiles of azimuthal Fourier modes of (ρu) obtained from FSM calculation of wake with central bleed jet; $I = 0.0038$, $I = 0.0113$, $I = 0.0226$ (from top to bottom); $z = 2.5$ (left) and $z = 7$ (right).

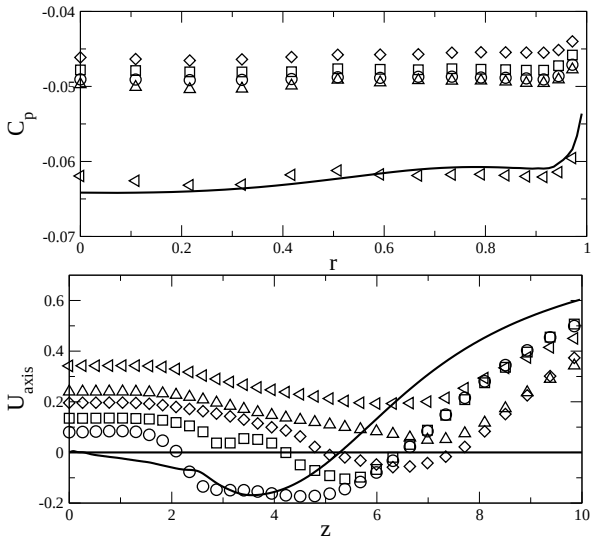

Figure 6.15 Pressure coefficient on base (top) and streamwise velocity along axis of symmetry (bottom) from FSM of basebleed; unforced case (—), $I = 0.0038$, ($\circ$), $I = 0.0075$, ($\square$), $I = 0.0113$, ($\diamond$), $I = 0.0148$, ($\triangle$), $I = 0.0226$, ($\triangleleft$).

modes $k = 1$, $k = 3$, $k = 4$ and $k = 6$ show high amplitudes compared to the natural wake indicating large disturbance amplification in the shear layer.

Radial distributions of the time-averaged pressure coefficient along the base and centerline distribution of the streamwise velocity for the wake with central bleed jet are shown in figure 6.15. As the injection parameter is increased the base pressure and recirculation length increases almost linearly. For $I = 0.0113$ the bleed flow provides most of the fluid required for shear-layer entrainment and the maximum base pressure is obtained. In the experiments of Mathur and Dutton[21, 22] peak performance was obtained for a higher value of the injection parameter. This can probably be attributed to a larger entrainment of fluid by the shear layer at the higher experimental Reynolds number.

7. Summary

We performed FSM simulations of transitional axisymmetric supersonic wakes at $M = 2.46$ and $Re_D = 100,000$. Active and passive flow control techniques were applied and it was demonstrated that the base-pressure can be increased by flow control. The effect of these flow control techniques on the flow structures and the mean flow was investigated. Consistent with the experiments at higher Reynolds numbers, applying steady forcing of higher azimuthal modes and generating longitudinal structures in the shear layer did not succeed in increasing the base pressure, except for a slight increase in pressure and recirculation length when steady forcing is applied to mode $k = 2$.

When applying periodic forcing of the axisymmetric mode, mode $k = 1$ is suppressed in the recirculation region and the amplitude of mode $k = 2$ is reduced in the shear layer. Forcing the axisymmetric mode at certain frequencies resulted in a base pressure increase and a longer recirculation length. In our simulations, a pressure increase was first observed for a non-dimensional frequency $\omega = 1.5$ and then for $\omega = 2.5$. This indicates an interesting trend and a strong dependence of the performance on the forcing frequency, which will be further investigated in the future.

We also investigated passive wake control using basebleed. In our preliminary simulations, the largest drag reduction (base pressure increase) was obtained for an injection parameter of $I = 0.0113$. This value is lower than the optimal injection parameter observed in the experiments. We attributed this to the higher experimental Reynolds number which leads to a stronger entrainment by the shear layer.

References

[1] Rollstin, L., "Measurement of inflight base-pressure on an artillery-fired projectile," *Journal of Spacecraft and Rockets*, Vol. 27, No. 1, 1990, pp. 5–6.

[2] Sandberg, R. D. and Fasel, H. F., "Instability mechanisms in supersonic base flows," *AIAA Paper 2004-0593*.

[3] Sandberg, R. D. and Fasel, H. F., "Numerical Investigation of Transitional Supersonic Axisymmetric Wakes," *J. Fluid Mech.*, Vol. 563, 2006, pp. 1–41.

[4] Sandberg, R. D. and Fasel, H. F., "Direct Numerical Simulations of Transitional Supersonic Base Flows," *AIAA J.*, Vol. 44, No. 4, 2006, pp. 848–858.

[5] Bourdon, C. J. and Dutton, J. C., "Planar visualizations of large-scale turbulent structures in axisymmetric supersonic separated flows," *Phys. Fluids*, Vol. 11, 1998, pp. 201–213.

[6] Bourdon, C. J. and Dutton, J. C., "Visualizations and measurements of axisymmetric base flows altered by surface disturbances," *AIAA Paper 2001-0286*.

[7] Sivasubramanian, J., Sandberg, R. D., von Terzi, D. A., and Fasel, H. F., "Numerical Investigation of Transitional Supersonic Base Flows with Flow Control," *Journal of Spacecraft and Rockets*, Vol. 44, No. 5, 2007, pp. 1021–1028.

[8] Forsythe, J. R., Hoffmann, K. A., Cummings, R. M., and Squires., K. D., "Detached-Eddy Simulation with compressibility corrections applied to a supersonic axisymmetric base flow," *Journal of Fluids Engineering*, Vol. 124, 2002, pp. 911–923.

[9] Sandberg, R. D. and Fasel, H. F., "Application of a new Flow Simulation Methodology for Supersonic Axisymmetric Wakes," *AIAA Paper 2004-0067*.

[10] Kawai, S. and Fujii, K., "Computational Study of Supersonic Base Flow Using Hybrid Turbulent Methodology," *AIAA J.*, Vol. 43, No. 6, June 2005, pp. 1265–1275.

[11] Rumsey, C. L., Gatski, T. B., and Morrison, J. H., "Turbulence Model Predictions of Strongly Curved Flow in a U-Duct," *AIAA J.*, Vol. 38, No. 8, August 2000.

[12] Sarkar, S., Erlebacher, G., Hussaini, M. Y., and Kreiss, H. O., "The Analysis and Modelling of Dilatational Terms in Compressible Turbulence," *J. Fluid Mech.*, Vol. 227, 1991, pp. 473–493.

[13] Sarkar, S., "The pressure-dilatation correlation in compressible flows," *Phys. Fluids A*, Vol. 4, No. 12, Dec. 1992, pp. 2674–2682.

[14] Speziale, C. G., "Modeling of Turbulent Transport Equations," *Simulation and Modeling of Turbulent Shear Flows*, Oxford University Press, New York, 1996.

[15] Durbin, P. A., "A Reynolds stress model for near wall turbulence," *J. Fluid Mech.*, Vol. 249, 1993, pp. 465–498.

[16] Sandberg, R. D., *Numerical investigation of transitional and turbulent supersonic axisymmetric wakes.*, Ph.D. thesis, The University of Arizona, 2004.

[17] Speziale, C. G., "A combined large-eddy simulation and time-dependent RANS capability for high-speed compressible flows," *Journal of Scientific Computing*, Vol. 13, No. 3, Sept. 1998, pp. 253–74.

[18] Fasel, H. F., Von Terzi, D. A., and Sandberg, R. D., "A Methodology for simulating compressible turbulent flows," *Proceedings of FEDSM'03*, 2003, 4th ASME/JSME Joint Fluids Engineering Conference, Honolulu, Hawaii, USA.

[19] Fasel, H. F., Seidel, J. J., and Wernz, S. H., "A Methodology for simulation of complex turbulent flows," *Journal of Fluids Engineering*, Vol. 124, 2002, pp. 933–942.

[20] Lewis, H. R. and Bellan, P. M., "Physical constraints on the coefficients of Fourier expansions in cylindrical coordinates," *J. Math. Phys.*, Vol. 31, No. 11, 1990, pp. 2592–2596.

[21] Mathur, T. and Dutton, C., "Base-bleed experiments with a cylindrical afterbody in supersonic flow," *Journal of Spacecraft and Rockets*, Vol. 33, No. 1, 1996, pp. 30–37.

[22] Mathur, T. and Dutton, C., "Velocity and turbulence measurements in a supersonic base flow with mass bleed," *AIAA J.*, Vol. 34, No. 6, 1996, pp. 1153–1159.

[23] Dubief, Y. and Delcayre, F., "On coherent-vortex identification in turbulence," *J. Turbulence*, Vol. 1, 2000, pp. 1–22.

[24] Sandberg, R. D. and Fasel, H. F., "Investigation of Supersonic Wakes Using Conventional and Hybrid Turbulence Models," *AIAA J.*, Vol. 44, No. 9, 2006, pp. 2071–2083.